Journal of Molecular Liquids 396 (2024) 124008

Contents lists available at ScienceDirect

Journal of Molecular Liquids

journal homepage: www.elsevier.com/locate/molliq

Antibacterial performance enhancement using hydrophobic deep eutectic solvents: COSMO-RS prediction, experimental validation, and synergistic action with antibiotics

Amal A.M. Elgharbawy [a,b,*], Huma Warsi Khan [c,h], Najihah Mohd Noor [a,b], Sharifah Shahira Syed Putra [d], Engku Normi Engku Ismail [a], Hanee Farzana Hizaddin [e], Maan Hayyan [f,*], Adeeb Hayyan [e,g], Wan Jefrey Basirun [d], Muhammad Moniruzzaman [h], Lama Al-afandi [a], Muhamad Shirwan Abdullah Sani [a]

[a] International Institute for Halal Research and Training (INHART), International Islamic University Malaysia, P.O Box 10, 50728 Kuala Lumpur, Malaysia
[b] Department of Chemical Engineering and Sustainability, Kulliyyah of Engineering, International Islamic University Malaysia, P.O Box 10, 50728 Kuala Lumpur, Malaysia
[c] Centre of Research in Ionic Liquids (CORIL), Universiti Teknologi PETRONAS, Seri Iskandar 32610, Perak, Malaysia
[d] Department of Chemistry, Faculty of Science, Universiti Malaya, 50603 Kuala Lumpur, Malaysia
[e] Department of Chemical Engineering, Faculty of Engineering, Universiti Malaya, 50603 Kuala Lumpur, Malaysia
[f] Chemical Engineering Program, Faculty of Engineering and Technology, Muscat University, P.O. Box 550, Muscat P.C. 130, Oman
[g] Sustainable Process Engineering Centre (SPEC), Department of Chemical Engineering, Faculty of Engineering, Universiti Malaya, 50603 Kuala Lumpur, Malaysia
[h] Chemical Engineering Department, Universiti Teknologi PETRONAS, 32610 Seri Iskandar, Perak, Malaysia

ARTICLE INFO

Keywords:
Green antibacterial agent
Ionic liquid
Bacterial infection
Antimicrobial resistance
Synergistic effect
Hydrophobic deep eutectic solvents

ABSTRACT

Microbial infection is a hazardous and challenging clinical problem that has attracted considerable attention recently, primarily owing to the noticeable rise in antimicrobial resistance. To address the medical requirements to encounter this dilemma, we present hydrophobic deep eutectic solvents (HDESs) that combine experimental research and computational prediction; conductor-like screening model for real solvents (COSMO-RS). Menthol-based HDESs were successfully obtained when mixed with fatty acids, and their thermal profiles were analyzed. The HDES systems and their synergistic effects demonstrated potent antimicrobial activity against Gram-positive and Gram-negative bacteria, with DES 4 (menthol:decanoic acid) exhibiting the highest bactericidal activity at a molar ratio of 1:5. The interaction between the HDESs and bacterial cell wall structural compounds was confirmed by field-emission scanning electron microscopy and Fourier transform infrared spectroscopy. The results revealed a favorable concurrence between the projected and empirical outcomes, indicating that DES 4 exhibited bacteriostatic properties and could be a viable substitute for managing bacterial infections of diverse origins. In addition, the synergistic effect of DES 4 and tetracycline showed promising potential. The successful integration of experimental and computational approaches in this study also sets a precedent for the rational design of future antimicrobial agents and opens new avenues for tackling other clinical challenges.

1. Introduction

Despite advancements in antimicrobial chemotherapy and supportive care, bacterial infections still pose significant risks for mortality and morbidity. Several factors, including poor prescription practices, lack of patient knowledge, and insufficient diagnostic resources, can cause antimicrobial resistance [1]. Immensely, due to the emergence of bacterial resistance, bacterial diseases remain a significant risk to the health of people, the environment, and animals.

Consequently, the pharmaceutical and food industries have shown great interest in natural compounds with antibacterial properties, owing to the recent discovery of different negative effects of conventional synthetic antimicrobials. Natural essential oils typically contain various natural antimicrobials, such as menthol, which are widely used. These

* Corresponding authors.
E-mail addresses: amalgh@iium.edu.my, amal.elgharbawy@gmail.com (A.A.M. Elgharbawy), maan_hayyan@yahoo.com, mhayyan@muscatuniversity.edu.om (M. Hayyan).

https://doi.org/10.1016/j.molliq.2024.124008
Received 15 September 2023; Received in revised form 12 December 2023; Accepted 8 January 2024
Available online 12 January 2024

substances are categorized as generally recognized as safe by the U.S. Food and Drug Administration, thus recognizing their broad applications in the food and pharmaceutical industries [2], although their use is subject to certain restrictions. However, the complexity of the components of natural antimicrobials, such as essential oils, should be considered. Notably, many natural antibacterial compounds have low solubility in water and high melting points, necessitating their proper dilution and dissolution by solvents or carriers.

Recently, deep eutectic solvents (DESs) have emerged as stable and environmentally friendly solubilization agents [3], and a promising solution to the aforementioned problems is using hydrophobic DESs (HDESs). HDESs typically comprise two or more hydrophobic solids that form a homogeneous liquid phase when mixed. The structural integrity of HDESs is maintained even in the presence of water due to their hydrophobicity, thus exhibiting minimal water uptake capacity and negligible leaching of their constituents into the aqueous phase [45]. This can be important for environmental and toxicological reasons because the leaching of solvent compounds into the aqueous phase can harm the environment and human health. Chen et al. [6] prepared HDESs composed of long-chain fatty acids (FAs) that were non-toxic, possessed better hydrogen bonding and were recyclable. These will also aid in following the principles of sustainable development goals, green innovation products, and ISO1400 [7,8]. Kongpol et al. [9] demonstrated that an HDES containing menthol and FAs could enhance the anti-inflammatory effects of curcumin. Silva et al. [10] investigated the biomedical potential of HDESs based on menthol and saturated FAs with varying chain lengths. They discovered that the combination of menthol and stearic acid demonstrated no significant cytotoxicity and enhanced wound healing properties, along with antibacterial effects against *Staphylococcus epidermis* and *Staphylococcus aureus* (*S. aureus*). Chen et al. [11] reported that, in FA-based HDESs, the loss of the HDES is the minimal cause of hydrophobicity. Hence, FAs and their derivatives were used in this study, and menthol was used as the base compound for the HDESs. DESs have been used in numerous biomedical studies to optimize the functionality of biological materials and improve the potency of active pharmaceutical ingredients. Several recent studies have focused on DESs with antibacterial activity, demonstrating their potential for therapeutic and preventive purposes as an antiseptic agent. Wang et al. [12] prepared benzalkonium chloride (BC) in a DES with acrylic acid (AA) or methacrylic acid (MA) for polymerization. The prepared BC-AA DES exhibited high antibacterial efficacy against *Candida albicans* and *S. aureus*. It was also reported recently that the acidic environment created by natural DESs (NADESs) damages the bacterium process; those containing acidic elements often have better antibacterial activities than neutral NADESs such as sugar-based NADES [13].

Hydrophilic DESs have several limitations that hinder their practical applicability, which include their preferential affinity toward polar compounds, irreversible precipitation of drugs, and elevated viscosity of most hydrophilic DES at ambient temperatures [14]. The wide range of FAs currently available for the formation of menthol-based HDESs [15] can lead to time-consuming laboratory experiments for identifying the most suitable solvents with optimal antimicrobial, interaction, and thermodynamic properties. An effective approach for simplifying this laborious process is to use a conductor-like screening model for real solvents (COSMO-RS), which is a non-empirical method used to calculate liquid–liquid equilibria [16]. COSMO-RS is a mathematical thermodynamic model that uses quantum chemistry to predict the thermodynamic properties of various mixtures [17]. COSMOtherm software with specific parameters was employed to perform the COSMO-RS simulations, making it an efficient tool for exploring and predicting the properties of different solutes and solvents. For instance, Rezaei Motlagh et al. [18] demonstrated the screening of ionic liquids (ILs) for the extraction of eicosapentaenoic acid. Li et al. [19] also utilized COSMO-RS to screen 195 ILs, comprising 15 anions and 13 cations, to produce antibacterial cellulose fibers. COSMO-RS has also been used for the extraction of antioxidants from rosemary [20] and formaldehyde separation [21]. Fallanza et al. [22] screened 696 room-temperature ILs for the separation of propane and propylene using COSMO-RS. Although numerous studies have investigated the antibacterial effects of various bacterial strains, a research gap concerning the prediction of the effectiveness of different types of FAs against these strains still exists.

To address the challenge of experimentally selecting HDES compositions, selected compounds to formulate HDESs were screened in this study using COSMO-RS. Then, the biological effects of selected and prepared HDESs on bacteria were investigated by evaluating the combined effects of FAs and menthol. The predicted results were experimentally verified. Hence, the objectives of this study were to: (1) screen menthol-based HDESs containing six different types of FAs (propionic, butanoic, hexanoic, octanoic, decanoic, and levulinic acids) in terms of their antibacterial properties; (2) test the selected HDESs through COSMO-RS against seven Gram-positive and seven Gram-negative bacterial strains via disc diffusion test (DDT), minimum inhibitory concentration (MIC), and minimum bactericidal concentration (MBC); and (3) further validate the results through synergistic action with general antibiotics using field emission scanning electron microscopy (FESEM) and Fourier transform infrared (FTIR) spectroscopy. The selected HDESs, which were formulated with natural antimicrobials, are expected to serve as innovative delivery systems for the utilization of natural antimicrobials in the food and pharmaceutical sectors.

2. Experimental section

2.1. Materials

Tetracycline and dimethyl sulfoxide (DMSO) with purity levels greater than or equal to 97 % were procured from R&M, a Swiss-based supplier. Analytical-grade menthol (Merck, Germany), propionic acid (≥99 %), butanoic acid (≥98 %), hexanoic acid (≥96 %), octanoic acid (≥98 %), decanoic acid (≥99 %), and levulinic acid (≥99 %) (Sigma-Aldrich, USA) for HDES preparation. The synthesis and analytical procedures were performed using deionized water.

2.2. Preparation of menthol-based HDESs

A combination of menthol and various FAs were added in specific amounts to prepare HDESs with different molar ratios (1:1,1:2,1:3,1:4, and 1:5) as presented in Table 1. The molar ratio was determined using the method reported by Tang et al. [23]. To prepare each HDES, the constituents were introduced into a sealed glass vessel and heated at 70 °C for a duration of 4 h, with no agitation. A uniform and lucid solution was expected to yield a promising HDES mixture. The mixture was then cooled to ambient temperature (25 ± 2 °C) prior to storage in a desiccator.

2.3. COSMO-RS computational methodology

The COSMO-RS prediction process involves two distinct steps. The initial stage entails generating virtual environmental conditions for the molecule using a continuous solvation model. Using quantum and chemical computations, a screening charge density, commonly known

Table 1
List of screened HDESs and their abbreviations.

HBA*	HBD*	Abbreviation
Menthol	Propanoic acid	DES 1
Menthol	Hexanoic acid	DES 2
Menthol	Octanoic acid	DES 3
Menthol	Decanoic acid	DES 4
Menthol	Butanoic acid	DES 5
Menthol	Levulinic acid	DES 6

* [24].

as sigma (σ), is assigned to each molecule. The distribution of screening charges on the surface of individual molecular species is converted into a σ-profile and σ-potential. These parameters can be utilized to discriminate between the molecular polarities and capacities of hydrogen bond donors and acceptors (HBDs and HBAs, respectively) and deduce the behavior of a given molecule upon its interaction with other components. The next step involves the use of statistical thermodynamics to calculate the energy of molecules due to interactions such as Coulomb repulsion, hydrogen bonds, and van der Waals forces. Based on COSMO-RS results, Hayyan et al. [25] reported that the aggregation of NADES species on the cellular membrane is crucial for their subsequent penetration into membrane layers. These specific species reportedly participate in electrostatic interactions with oppositely charged groups that are present on the membrane, leading to the eventual puncturing of the bilayer. Therefore, collecting sufficient data regarding this phenomenon is essential to validate our prior hypothesis and determine whether this mechanism is analogous in both NADESs and DESs.

At the outset, each compound subjected to chemical structure analysis was drawn and refined using the Hartree–Fock level and 6-31G* basis set. The TURBOMOLE program (TMole-X) was used to generate a COSMO file for each structure. The optimization process was performed using a single-point calculation approach within the framework of density functional theory at the triple-zeta valence potential (TZVPD) basis set level. COSMOlogic suggests the use of BP-TZVPD-FINE for improved accuracy in forecasting thermophysical characteristics because it employs a more comprehensive TZVPD basis set. Subsequently, the cosmo files were imported into the COSMOthermX software package.

Table 2 presents the abbreviations of phosphatidylethanolamine, N-acetyl-alpha-neuraminic acid, and N-acetylglucosamine used in this study as cell membrane components.

2.4. Representation of HDESs in COSMOtherm-X

DESs have been identified as environmentally friendly alternatives to conventional solvents. Moreover, these are similar, with a slight difference in the components used. HDESs screening using COSMOthermX was performed. Three approaches are available, namely, electroneutral, metafile, and segmented or fragmented approaches, which are used to represent ILs in the COSMO software [26]; the electroneutral method is commonly used to screen ILs [27]. Because of the resemblance in their compositional structures, the electroneutral method was selected for the depiction of the DESs in COSMO-RS, namely HBA and HBD, as determined by their mole composition [28].

The evaluations were performed using the COSMOtherm software (18.0.2 version), and the thermodynamic properties were determined by BP_TZVP-C30_1201 parameterization. The σ-surfaces and σ-profiles were obtained using the COSMOtherm software. Fig. 1 shows a step-by-step schematic representation of the COSMO-RS screening. These profiles were used to determine molecular interactions. The σ-profiles of HDESs and FAs were evaluated using Eq. (1) [29]:

$$P(\sigma) = \sum_{i}^{N} x_i p_i(\sigma) \tag{1}$$

where i is the concentration of DES/FAs.

For effective application of this methodology, changing the mole fractions obtained via COSMO-RS is essential to precisely reflect the experimental definition of the mole fraction. The aforementioned task can be accomplished using mathematical expressions as follows: Eq. (2) provides an experimental representation of the mole fraction of the solute present in a solution comprising the solute, carrier, and DES.

$$x_{i_{EXP}} = \frac{n_i}{n_i + n_j + n_{DES}} \tag{2}$$

In COSMOthermX, the definition of mole fraction is given by Eq. (3).

$$x_{i_{COSMO-RS}} = \frac{n_i}{n_i + n_j + n_{HBA} + n_{HBD}} \tag{3}$$

where $x_{i_{EXP}}$ is the experimentally determined mole fraction of solute i,$x_{i_{COSMO-RS}}$ is the mole fraction of solute i in COSMO-RS, n_i is the number of moles of solute i, n_j is the number of moles of carrier j, n_{DES} is the number of moles of DES, n_{HBA} is the number of moles of HBA in DES, and n_{HBD} is the quantity of moles of HBD in DES.

Eq. (1) and (2) can be simplified further to Eq. (3) to convert the calculated mole fraction of COSMOthermX into the experimental definition, as shown in Eq. (4).

$$x_{i_{EXP}} = \frac{x_{i_{COSMO-RS}} / v_i}{\sum_k x_{k_{COSMO-RS}} / v_k} \tag{4}$$

where the stoichiometric coefficient of each component is denoted by v_i.

2.5. Preparation of bacterial cultures

Bacterial isolates (Table S1) derived from Gram-positive bacteria *B. subtilis* ATCC11774 (MYP agar) and *S. aureus* ATCC 12600 (mannitol agar) and Gram-negative bacteria *E. coli* ATCC 1129 (EMB agar) were retrieved from a 4 °C freezer through the utilization of blood agar media. Initially, the three bacterial species were pre-cultured. The experiment involved inoculating 10 mL of autoclaved tryptone soy broth (TSB) with a loopful of cells followed by incubation at 37 °C for 24 h.

2.6. Assessment of antibacterial activity

2.6.1. Determination of disc diffusion test (DDT)

Sterile cotton buds were used, and the cells were evenly distributed on the plates containing a medium solidified with agar. A sterile filter paper (Whatman No. 1) with a diameter of 6 mm was immersed in different HDES solutions and allowed to equilibrate. The filter paper was incubated with the seeded discs. Subsequently, the discs were incubated at 37 °C for 24 h. The diameters of the inhibition zones were then measured. The analysis was performed in triplicate for each bacterial strain [30]. The experimental protocol involved the use of 5 mg mL^{-1} as the positive control and DMSO as the negative control, as reported previously [10]. DMSO was used as the negative control to dilute tetracycline.

2.6.2. Determination of MIC and MBC

A broth microdilution assay was used to investigate the antibacterial properties of the DESs. This involved the implementation of a sequential microplate dilution method using sterile 96-well plates, as described by Abakar et al. [31]. Approximately 0.1 mL of sterilized TSB was added to each row. Wells 2 to 11 were replenished with 0.1 mL of HDES and then subjected to serial dilutions with prefilled TSB, resulting in concentrations ranging from 500 mg mL^{-1} to 0.5 mg mL^{-1}. The initial well functions as a mechanism for growth regulation. Subsequently, a volume of 0.01 mL of the culture medium containing the HDES was introduced to each well. The deep wells were incubated at 37 °C for 24 h. Turbidity was evaluated during the incubation period, specifically at T = 0 and T = 24 h, by measuring the optical density at 600 nm (ODλ = 600) using a microplate reader (Thermo Fisher Scientific Multiskan™ GO spectrophotometer, Finland). The experiments were conducted in triplicate for each assay. The MIC was determined by identifying the lowest

Table 2
List of cell membrane components used in computational screening (COSMO-RS) and their abbreviations.

Component	Abbreviation
Phosphatidylethanolamine	PE
N-Acetyl-alpha-neuraminic acid	NAC
N-Acetylglucosamine	AGA

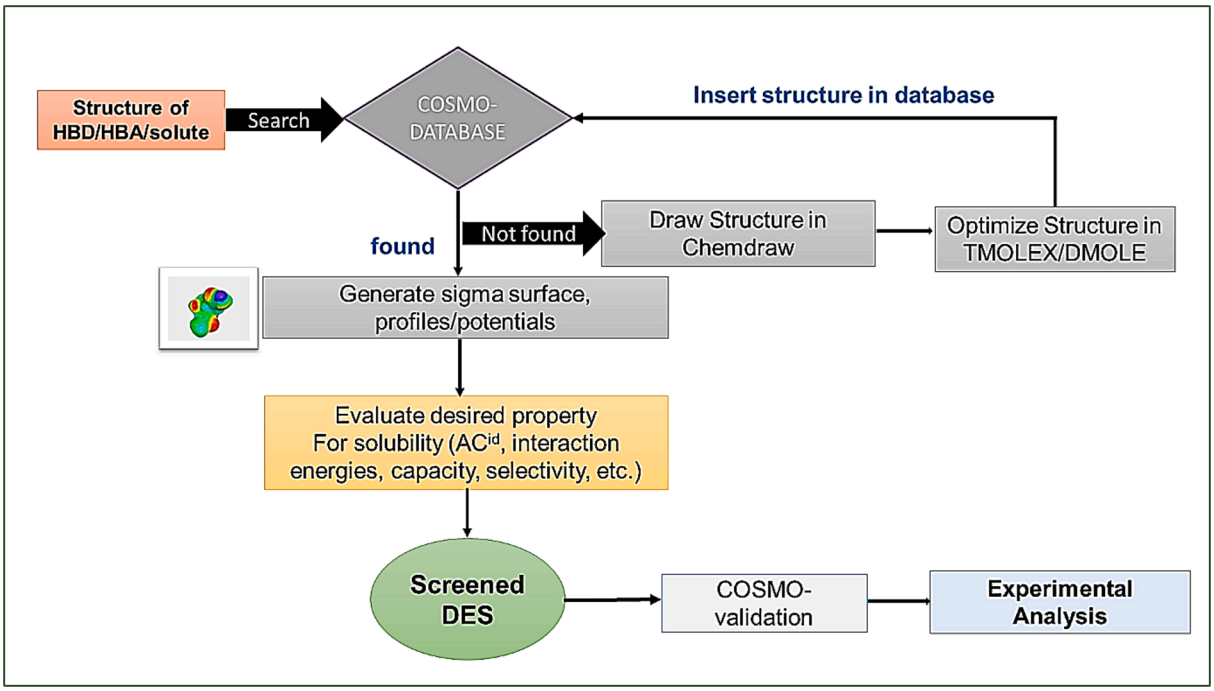

Fig. 1. Step-by-step representation of conductor-like screening model for real solvents (COSMO-RS) screening.

concentration of the synthesized compounds that resulted in discernible inhibition of bacterial growth. A quantity from each well that was equal to or greater than the MIC was streaked on Mueller–Hinton agar, as it supports a satisfactory majority of bacterial pathogen growth and acts as a tetracycline inhibitor. Each well was incubated at 37 °C for one day to calculate the MBC. Each determination was performed in triplicate. The MBC was chosen on plates with concentrations that did not grow.

2.6.3. Synergistic effect of HDESs for antibacterial activity

A synergistic assessment was performed to examine the antimicrobial activity of the DESs in enhancing antibiotics: tetracycline (tetracycline hydrochloride, Fischer Scientific, USA), ampicillin (sodium salt, Gold Biotechnology, USA), and penicillin G (sodium Salt, Gold Biotechnology, USA). For this experiment, the MIC results (Section 3.3.2) were used as the parameters for evaluation.

The test was conducted by filling 200 μL of antibiotic (12.5 mg mL^{-1}) in the first well on the first row. Next, the second well onwards of the first row was filled with 100 μL of DMSO. Each well was then serially diluted, and a volume of 100 μL from the last well was discarded. Then, the second row of the wells was filled with 20 μL of 106 CFU mL^{-1} bacterial suspension to prepare an antibiotic concentration ranging from 10 to 0.01 μg mL^{-1} (two references). A microtiter plate was incubated at 37 °C for 24 h, and the optical density was then measured at 600 nm (Thermo Scientific™ Multiskan™ GO microplate spectrophotometer). The synergistic test was performed in four sets of MIC tests. These tests were conducted by adapting two parameters: (1) the concentration of the lowest MIC value of DES 3 and DES 4 from the MIC results (Section 3.3.2) against selected bacterial strain and (2) the concentration of the lowest four MIC values of antibiotic concentration based on the aforementioned antibiotic screening test. This synergistic MIC test was conducted using the same method as that described previously (Section 2.6.2).

2.7. Fourier transformed infrared (FTIR) spectroscopy analysis

The spectra of the HDES and samples (bacteria, bacteria treated with DES, and bacteria treated with HDES and antibiotics) were obtained using a PerkinElmer Spectrum 400 FTIR spectrometer (Perkin Elmer, USA). Approximately, 0.1 g of samples of functional groups were evaluated for alterations. To collect the single-beam spectra of the samples, 32 scans were conducted with a resolution of 4 cm^{-1} and at a scanning range of 500–4000 cm^{-1}.

2.8. Examination of the antimicrobial activity by field emission scanning electron microscopy (FESEM)

The antimicrobial activity toward DES 4 AND DES 4/antibiotics was examined using FESEM. Three samples of *S. aureus* were prepared (*S. aureus*, *S. aureus* treated with DES 4, and *S. aureus* treated with DES 4 and tetracycline) and incubated at 37 °C for 24 h before testing. Approximately, 10 μL of the specimens were applied onto a glass coverslip and desiccated under ambient conditions. The specimens were air-dried and subsequently coated with a blend of gold and palladium alloys via sputtering. The samples were then examined by FESEM at an accelerating voltage of 5 kV.

2.9. Statistical analysis

The samples were prepared in triplicate and Microsoft Excel (Microsoft Office Excel, 365) was used for statistical analysis. For at least 10 measurements, bar charts present the data in terms of mean and standard error. A statistically significant difference was established at $p < 0.05$.

3. Results and discussion

3.1. σ-Surfaces and σ-Profiles for cell membrane components and HDESs

PE is a predominant lipid found in organelles and cell membranes and plays a crucial role in maintaining membrane integrity [32]. Being a neutral aminophospholipid, it exhibits a diverse range of interactions, including its distinct capability to function as a molecular chaperone [33]. However, sialic acid-cleaving enzymes, known as NAC, are expressed in a diverse array of organisms, including pathogens. Sialic acids are monosaccharides with a wide range of structural variations found in nature [34]. Additionally, AGA is abundant in the cell walls of

fungi and certain algae, as well as in the cuticles or exoskeletons of numerous invertebrates [35]. Owing to their significant involvement in diverse biological processes, PE, NAC, and AGA were chosen as the cell membrane constituents of interest for this study. Initially, the σ-surfaces and σ-profiles of the cell membranes (PE, NAC, and AGA) were generated using COSMO-RS.

In this section, the validation of the COSMO-RS-predicted results is evaluated through comparison with experimental data for different menthol-based HDESs. The COSMO-RS model was used to examine the chemical interactions and assess the ability of HDESs to dissolve cell membranes, thereby acting as antibacterial agents.

Subsequently, the σ-profiles and σ-surfaces were calculated for the HDES compounds to gain insights into their chemical characteristics, which are a valuable tool for predicting the thermodynamic properties of chemical entities. The results revealed that the σ-surfaces of PE, NAC, and AGA possessed positively and negatively charged groups. The blue color indicates the presence of an NH group that donates electrons and is positively charged [36]. Red indicates the presence of O^{-}, which accepts protons and hence acts as an HBA [37], green signifies the neutral behavior caused by the presence of carbon, and blue signifies a neutral region. Fig. 2 shows the σ-surface for (a) PE, (b) NAC, and (c) AGA. The results revealed that all FA derivatives (FADs) possessed positive, negative, and neutral sites and hence behaved as HBD and HBA.

Subsequently, the σ-potentials and σ-profiles of PE, NAC, and AGA were evaluated, and the results revealed that all cell membranes behaved as HBA. A series of peaks were observed in both the HBA and HBD regions. The peaks in the positive region can be attributed to the presence of O^{-} groups, which can accept protons and provide stabilization [17]. The positive peaks in the positive region indicate the presence of an NH group, which is a substantial donor that becomes positively charged. Positive values indicated a higher occurrence of repulsive interactions, whereas negative values indicated a significantly greater level of interaction between molecules [38]. The intensities of the peaks of PE, NAC, and AGA differed depending on the molecular structure. The order of the peaks shows the following trend:

$$\text{HBD region}: \ \text{NAC} > \text{AGA} > \text{PE}$$

$$\text{HBA region}: \ \text{AGA} > \text{NAC} > \text{PE}$$

$$\text{Non}-\text{polar region}: \ \text{PE} > \text{NAC} = \text{AGA}$$

The results (Fig. 3) reveal that HBDs and HBA possess both polar and non-polar sites. However, hexanoic aid, decanoic acid, hexanoic acid, and butanoic acid cause of the COOH group are more hydrogen bond acceptors. Propionic acid, octanoic acid, decanoic acid, hexanoic acid, levulinic acid, and butanoic acid will behave as HBA and hence will form a bond with HBD via synergism. Small peaks can also be observed in the HBD region, signifying a smaller hydrogen bond-donating nature. The individual sigma profiles reveal that HBD and HBA will form bonds with each other, resulting in the formation of DES.

The σ-potentials (Fig. 4) were then evaluated, signifying interactions

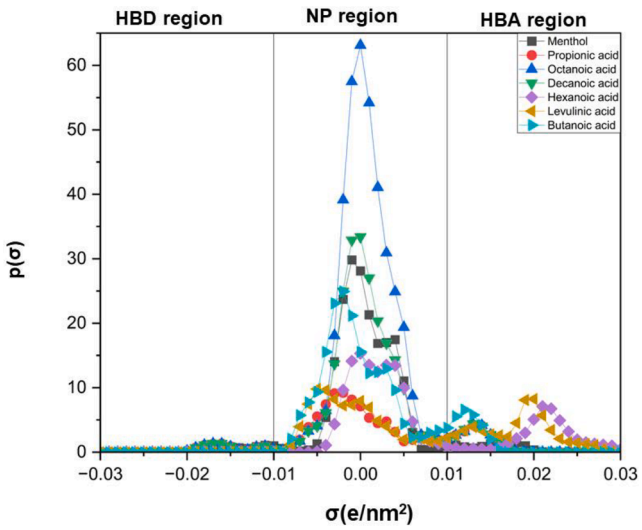

Fig 0.3. σ-profiles for HBD and HBA understudy.

between the HBD and HBA. In the HBD regions (Fig. 4a), peaks were observed at −0.0175, −0.015, and −0.013 e/nm^2 for NAC, AGA, and PE, respectively. Similarly, a series of peaks in the HBA region was observed at 0.015 e/nm^2 for all FADs (NAC, AGA, and PE). The peak intensity of PE was lower than that of NAC and AGA, indicating that NAC and AGA exhibited higher electronegativity because of their highly electronegative nature [39]. Consequently, NAC, AGA, and PE exhibited the HBA behavior as seen in Fig. 4b. Considering the higher peak intensity in the HBA region observed in the σ-profile, these cell membranes were expected to serve as more effective HBAs [40]. Although the choice of HBA in the cell membrane has a significant impact, the selection of a hydrophobic HBD can also have a synergistic effect [20]. Because the cell membrane comprises functional groups or molecules that can serve as HBDs, they can be attracted to HBAs. Hence, HBAs in the cell membrane interact with and possibly stabilize HBA by forming hydrogen bonds with HBDs from other molecules or structures.

3.2. Molecular interaction with the selected DES

To determine the molecular interactions of NAC, AGA, and PE with the HDESs, σ-profiles of the selected HDES and FADs were plotted (Fig. 4). This provides insight into the of interaction of DESs with FADs [41]. In addition to the molecular structure, the molar ratio also plays an essential role. Initially, different molar ratios, namely 1:1, 1:2,1:3,1:4, and 1:5 were used as the ratio of HBD:HBA for all examined DESs. Typically, DESs consist of three components: salt cations, anions (HBA), and HBD, and determining a symmetrical curve at 0 e/nm^2 to the right peak of the membrane is favorable for the interaction to occur in the nonpolar region.

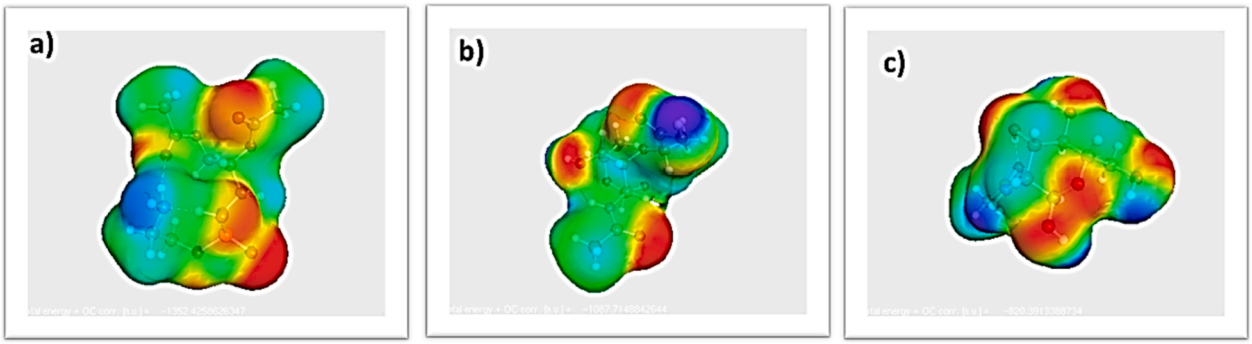

Fig. 2. σ-Surfaces of (a) phosphatidylethanolamine (PE), (b) N-acetyl-alpha-neuraminic acid (NAC), and (c) N-acetylglucosamine (AGA).

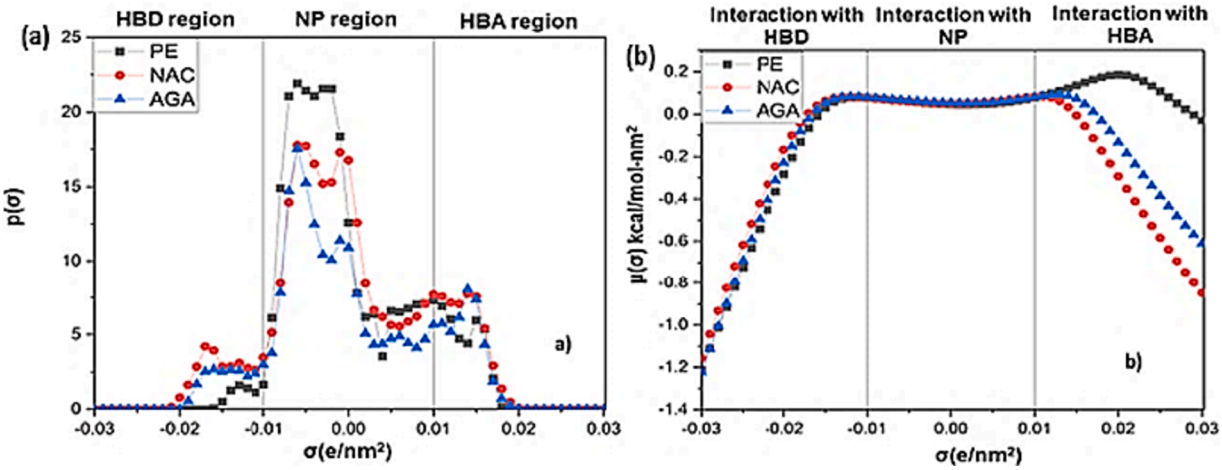

Fig. 4. (a) σ-profile (b) σ-potential; interaction between hydrogen bond donors (HBDs) and hydrogen bond acceptors (HBAs) for all three fatty acids (PE, NAC, and AGA) using COSMO-RS.

Fig. 5a shows the characteristics (σ-profiles) of DESs (DES 1 – DES 5) and FADs (fatty acid derivatives). DESs have both polar and nonpolar features. The HBD is vital for the positive charge density in nonpolar regions of membranes. Peaks in the range of $0 < \sigma < 0.01$ e/nm^2 (right side of the profile) interact with the left peaks of membranes (-0.006 eA^2 for PE, NAC, and AGA). All DESs exhibit peaks within these ranges. Noteworthy, DES 4 has the highest peaks among all DESs, both at positive and negative σ values. At −0.001 e/nm^2, DES 4 has the highest peak due to the longer carbon chain in its decanoic acid compared to other HBDs. These findings suggest that saturated long-chain fatty acids demonstrate more compatibility in the interaction between DESs and membranes when compared to their short-chain counterparts [42]. Additionally, DES 3 also stands out with higher peaks that align with all three membranes. This suggests strong interactions between DESs and membranes, enabling effective penetration. DES 2 exhibits a clear preference for interaction, particularly with NAC and AGA, highlighting a distinct affinity. Similarly, DES 5 displays an inclination for interaction with NAC and AGA, especially at elevated molar ratios. In contrast, DES 1 demonstrates a notable absence of interaction with PE, NAC, and AGA, even when molar ratios are increased, reinforcing the specificity and selective nature of the interaction pattern observed [42].

The computational analysis indicated that DES 3 and DES 4 at a molar ratio of 1:5 demonstrated greater interactions with membrane components. Further insights were gained from the analysis of the σ-potential, which revealed that as the molar ratio increased, the number of molecular interactions also increased, as indicated by higher σ-potential values in the HBA region. This was particularly evident in the case of DES 4, where the optimal interaction was observed at a molar ratio of 1:5, indicating that the molar ratio 1:5 was the most effective for DES 4 in terms of potential interactions with bacterial membrane components. Other tested molar ratios, including 1:2, 1:3, 1:4, and 2:1 did not exhibit as strong interactions as the 1:5 ratio, suggesting a lower potency for antibacterial activity (**Fig S1 and S2**).

The selection of the HDES was significantly influenced by the molar ratio. To explore the impact of varying the molar ratio, the σ-potential of DES 4 is plotted in Fig. 5b. Initially, the peak intensity was low at a molar ratio of 1:1. However, as the molar concentration increases, the peak intensity increases. The maximum peak intensity was observed at the molar ratio of 1:5. Nevertheless, a further increase in the molar ratio decreased the peak intensity. The minimum peak intensity was observed at the molar ratio of 1:1. This indicates that at a molar ratio of 1:1, there is less interaction between DES 4 and the cell membranes. This can be attributed to excess HDES compared to the cell membranes, leading to the formation of a smaller complex. As the molar ratio increased, the number of molecular interactions also increased, as indicated by the higher σ-potential values in the HBA region. However, with a further

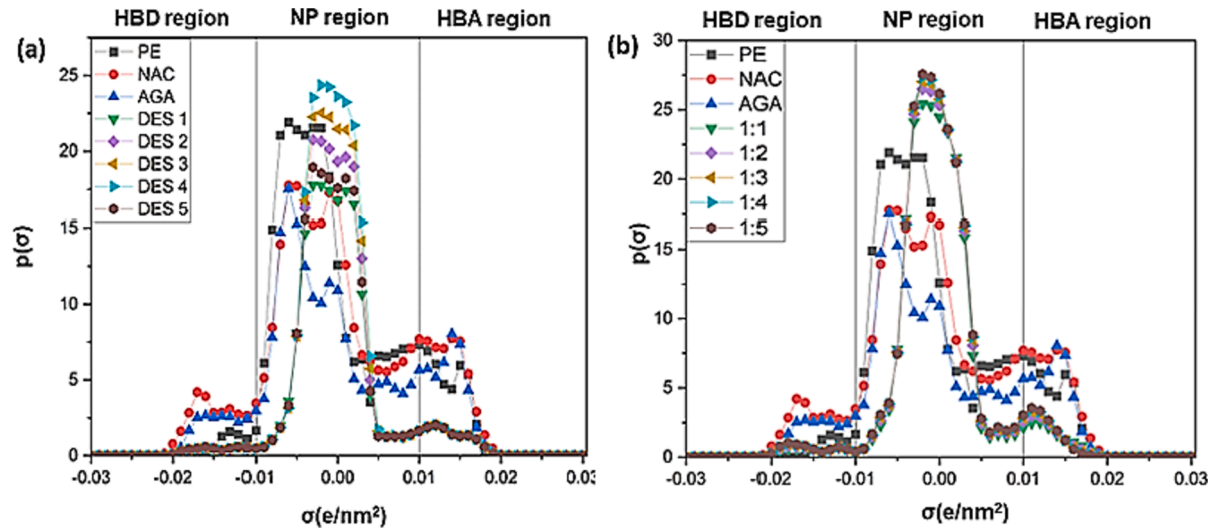

Fig. 5. σ- profiles of (a) HDESs and (b) DES 4 at different molar ratios using COSMO-RS.

increase in the molar ratio, the σ-potential values began decreasing, suggesting reduced exchange between molecules [43]. Based on these findings, a molar ratio of 1:5 for DES 4 was chosen.

To further investigate the molecular interactions, the σ-potential was examined, as illustrated in Fig. 6. In the σ-potential plot, a higher positive value indicates a more repulsive behavior, whereas a higher negative value signifies an increasing interaction between the molecules. The horizontal axis provides insights into the intricate network of interactions between the HBDs and HBAs. The interaction between the HBDs was reflected in the decrease of the hydrogen-bonding threshold (0.0084 e/nm^2). Notably, the positive values of the curves in the non-polar region indicated the high potential of the DESs. The DESs and membranes exhibited similar patterns, suggesting that interactions occurred within the mixture. These results indicated that DES 4 demonstrated stronger interactions with PE, NAC, and AGA than other HDESs. The results from these experiments, which demonstrated a significant zone of inhibition around the antibacterial agent-impregnated discs, further validated our choice of DES 3 and DES 4 at the specific molar ratio. Therefore, the decision to focus on DES 3 and DES 4 with a molar ratio 1:5 was based on a combination of COSMO-RS predictions and σ-potential analysis, which were subsequently validated through experimental assays in the following sections.

3.3. Validation of COSMO-RS simulation results

3.3.1. Disc diffusion test (DDT) and controls against bacterial strains

Based on the COSMO-RS prediction in selecting an ideal DES as a greener antibacterial agent, DES 3 and DES 4, with a molar ratio of 1:5 M, were further validated for their antibacterial activity owing to their greater interactions with PE, NAC, and AGA. Antibacterial activity was assessed using the Kirby–Bauer DDT, and the diameter of the zone of inhibition was measured. The DESs were utilized to produce outcomes against 14 bacterial strains (7 Gram-positive and 7 Gram-negative bacteria). This method creates a concentration gradient around the antibacterial agent-impregnated disc to identify resistant bacteria. A gradient of the antibacterial agent inhibited the germination and growth of the tested bacteria, forming a zone of inhibition around the disc, as shown in Fig. 7. The inhibition zone measurements of Gram-positive bacteria are presented in Table 3.

The results in Table 3 show that both HDESs possess antibacterial activity, as inhibition zones are observed for all the tested bacteria. As a constituent, menthol demonstrated varying levels of antibacterial activity across different bacterial strains. While its overall efficacy was lower compared to that of DES 3 and DES 4, menthol did exhibit notable activity, particularly against *S. pneumoniae*. This suggests that while menthol contributes to the antibacterial properties of HDESs, its effectiveness is significantly enhanced when synergistically combined with other components in the HDES formulation. The antibacterial impact of octanoic acid was observed to be moderately effective. Its capability, especially in inhibiting *B. subtilis* and *L. monocytogenes*, signifies its valuable contribution to the effectiveness of HDES formulations. This moderate antibacterial action of octanoic acid may be linked to its relatively shorter alkyl chain when compared to decanoic acid, hinting at a possible relationship between the length of the alkyl chain and the degree of antibacterial strength. In contrast, decanoic acid demonstrated a more pronounced antibacterial effect, especially against strains like *S. aureus and L. monocytogenes*. This observation is in harmony with the research by Watanabe et al. [44], which suggests a direct relationship between the lengthening of fatty acid chains and increased antibacterial activity. The enhanced effectiveness of decanoic acid, particularly evident in its role within DES 4 against *L. monocytogenes*, accentuates its crucial contribution to the heightened antibacterial capability of the solvent.

Overall, DES 4, with decanoic acid as a hydrogen donor, showed better inhibitory properties against all tested gram-positive bacteria, with the largest inhibition zone of 19 mm against *L. monocytogenes,* compared to DES 3. As stated earlier, these results are in agreement with those reported by Watanabe et al. [44] that the antibacterial activity is

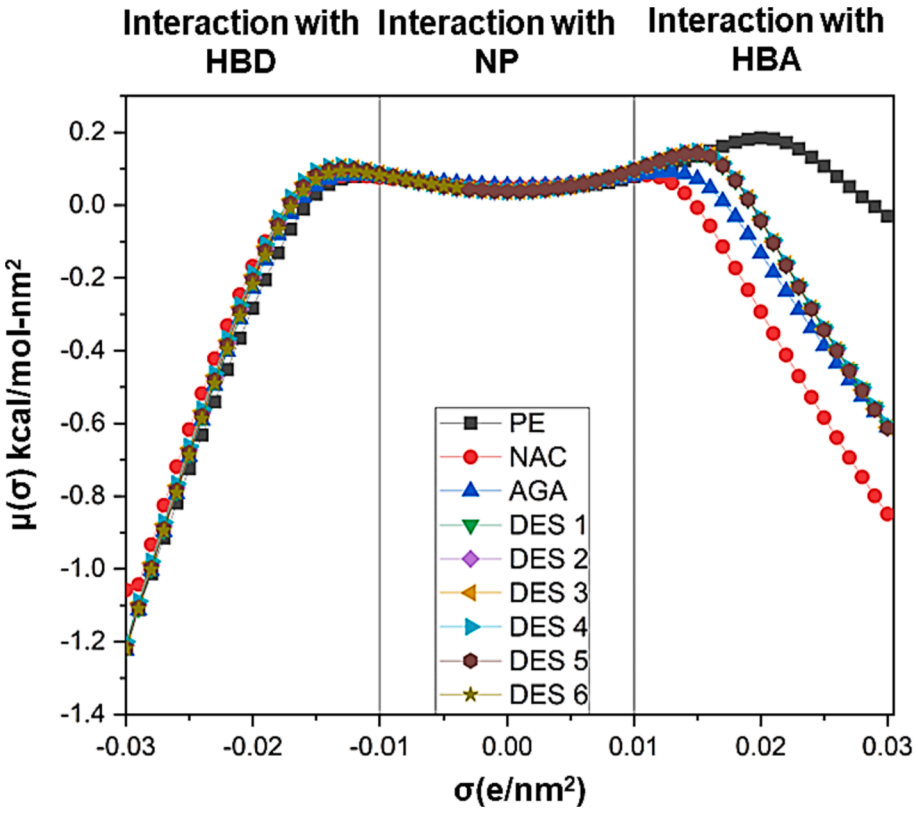

Fig. 6. σ-Potential verification for HDESs (DES 1–6) and cell membranes (PE, NAC, and AGA) using COSMO-RS.

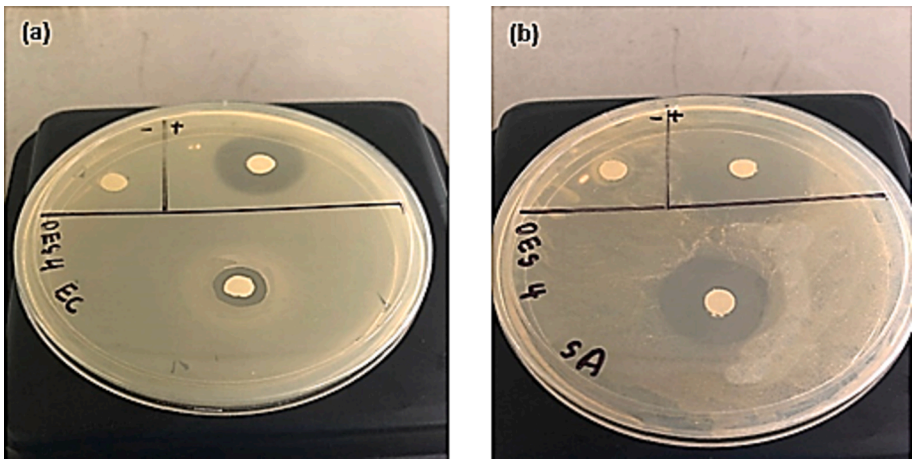

Fig. 7. Representative inhibition zone assay of DES 4 against (a) *Escherichia coli (E. Coli)* and (b) *Staphylococcos aureus (S. aureus)*.

Table 3
Disc diffusion test of DESs against Gram-positive bacteria.

DES/ Compound	Inhibition zone on Gram-positive bacteria [1,2,3,4,5] (mm)						
	C. diphtheria	*S. pneumoniae*	*B. subtilis*	*S. aureus*	*L. monocytogenes*	*B. cereus*	*C. perfringens*
DES 3	16.0 ± 0.0	14.5 ± 0.7	11.5 ± 0.7	20 ±0. 0	16.5 ± 0.7	12.5 ± 0.7	18.5 ± 0.7
DES 4	15.0 ± 0.0	16.0 ± 0.0	17.0 ± 0.0	18 ±0. 0	19.0 ± 0.0	15.5 ± 0.7	14.5 ± 0.7
Menthol	10.0 ± 0.0	25.0 ± 0.0	10.0 ± 0.0	10 ± 0.0	12.0 ± 0.0	18.5 ± 0.7	20.0 ± 0.0
Octanoic acid	14.0 ± 0.0	12.0 ± 0.0	15.5 ± 1.4	13.5 ± 0.7	16.5 ± 0.7	9.5 ± 2.1	11.5 ± 0.7
Decanoic acid	10.5 ± 0.7	14.5 ± 0.7	12 ± 0.0	17.5 ± 0.7	17.0 ± 0.0	14.5 ± 0.7	12.5 ± 0.7
Positive control	25.0 ± 0.0	13.5 ± 0.7	26.0 ± 1.4	28.0 ± 1.4	29.5 ± 0.7	17.5 ± 0.7	25.0 ± 0.0
Negative control	NI	NI	NI	NI	NI	NI	NI

[1] Values are expressed as mean inhibition ± SD (n = 2).
[2] NI - No inhibition
[3] Tetracycline hydrochloride was used as the positive control.
[4] Dimethyl sulfoxide (DMSO) was used as the negative control.
[5] Slight antimicrobial activity (inhibition zone of sample 1——3 mm), Moderate antimicrobial activity (inhibition zone of sample 3——4 mm), Clear antimicrobial activity (inhibition zone of sample 4——10 mm), Strong antimicrobial activity (inhibition zone of sample > 10 mm).

positively correlated with the elongation of the alkyl chain. DES 3 showed antibacterial activity comparable to that of DES 4, with the highest inhibitory activity against *S. aureus*. FAs and FADs demonstrated selective bactericidal activity and preferentially inhibited *S. aureus*; hence, a large inhibition zone was observed around the disc impregnated with DES 3. According to Yoon et al. [30], membrane destabilization and pore formation can be attributed to the amphipathic properties of antimicrobial lipids. The destabilization of the membrane results in enhanced cell permeability and lysis, thereby hindering the proliferation of bacterial cells, which can have either a bacteriostatic or bactericidal effect.

Similarly, DES 4 showed better inhibitory activity against all the tested Gram-negative bacteria than DES 3, as shown in Table 4. Unlike the inhibitory efficacy of both HDESs against Gram-positive bacteria, Gram-negative bacteria exhibited superior resilience to antibacterial activity owing to their intricate membrane construction. The lipopolysaccharides in the outer membrane of the cell wall act as barriers to permeability, thereby impeding the penetration of the HDESs into the cell membrane and their consequent impact. Conversely, Gram-positive bacteria possess thick and porous peptidoglycan layers in their cell walls, which facilitate the penetration of HDESs. This enables HDESs to interact with peptidoglycans before disrupting the lipid membranes of

Table 4
Disc diffusion test of HDESs against Gram-negative bacteria.

DES/ Compound	Inhibition zone on Gram-positive bacteria [1,2,3,4,5] (mm)						
	S. sonnei	*S. typhi*	*S. enteritidis*	*E. coli*	*P. mirabilis*	*V. parahaemolyticus*	*V. vulnificus*
DES 3	8.0 ± 0.0	10.0 ± 0.0	10.0 ± 0.0	9.0 ± 1.4	13.5 ± 0.7	13.5 ± 0.7	13.5 ± 0.7
DES 4	12.5 ± 0.7	19.0 ± 8.9	11.0 ± 0.0	9.0 ± 0.0	19.0 ± 1.4	12.5 ± 0.7	16.0 ± 0.0
Menthol	NI	8.5 ± 0.7	8.0 ± 0.0	NI	12.5 ± 0.7	12.5 ± 0.7	12.0 ± 0.0
Octanoic acid	10.0 ± 0.0	8.5 ± 0.7	9.0 ± 0.0	9.0 ± 0.0	14.5 ± 0.7	15.5 ± 0.7	12.5 ± 0.7
Decanoic acid	8.0 ± 0.0	8.0 ± 0.7	9.5 ± 0.7	7.0 ± 0.0	11.5 ± 0.7	11.5 ± 0.7	11.0 ± 1.4
Positive control	23.5 ± 0.7	24.5 ± 0.7	26.0 ± 1.4	23.5 ± 0.7	26.0 ± 0.0	24.5 ± 0.7	25.0 ± 0.0
Negative control	NI	NI	NI	NI	NI	NI	NI

[1] Values are expressed as mean inhibition ± SD (n = 3).
[2] NI - No inhibition
[3] Tetracycline hydrochloride was used as the positive control.
[4] DMSO was used as the negative control.
[5] Slight antimicrobial activity (inhibition zone of sample 1——3 mm), Moderate antimicrobial activity (inhibition zone of sample 3——4 mm), Clear antimicrobial activity (inhibition zone of sample 4——10 mm), Strong antimicrobial activity (inhibition zone of sample > 10 mm).

Gram-positive bacteria through hydrophobic interactions with the hydrophobic alkyl chain of the DES [10,45]. Each bacterium has a different level of resistance toward antibacterial agents, even if it belongs to the same species. The ability of certain bacteria to alter the hydrophobicity of their cell surface may explain the varying responses of different strains of the same species to antibacterial actions.

Both HDES formulations in this study exhibited enhanced antibacterial efficacy relative to their respective individual counterparts owing to the supramolecular organization between the two constituents in the HDES form. This results in a synergistic or additive effect, thereby rendering the HDES more or less cytotoxic than the individual constituents [10,46]. These results were in good agreement with the COSMO-RS prediction based on the interaction of selected components of cellular membranes, despite the fact that the model did not precisely replicate the composition found in the actual sample, particularly in relation to the ratio and frequency of the functional groups.

3.3.2. MIC and MBC against Gram-negative and Gram-positive bacteria

An exhaustive examination of the antibacterial effects of HDESs and their singular constituents was thoroughly conducted via MIC and MBC tests. These tests are essential in qualitatively evaluating the level of bacterial resistance or vulnerability to these substances. Detailed insights into the MIC and MBC figures for the HDESs and their separate components, against a suite of 14 bacterial varieties, are systematically compiled in Table 5.

The data in Table 5 describe the MIC and MBC metrics and illuminate the varying degrees of antibacterial efficacy exhibited by the HDESs. A notable observation was the significant antibacterial action of DES 3 and DES 4 across all the concentration levels tested. Particularly striking was their activity at the minimal concentration level (0.044 mg mL^{-1}), where they outperformed the antibacterial effects of menthol, octanoic acid, and decanoic acid against all bacterial samples tested.

The MIC tests, which are crucial for determining the lowest concentrations that inhibit bacterial growth, were aptly augmented by the MBC tests. The MBC tests played a key role in ascertaining the least concentrations required to eradicate 99.9 % of bacterial presence within a 24-hour timeframe [30]. Although the MBC readings were largely uniform across the different bacterial strains, B. cereus and C. perfringens stood out with MBC values that were higher than the MIC ones, indicating a variegated bactericidal response.

These results are in sync with the predictions made by the COSMO-RS model, as touched upon in earlier discussions in Section 3.2. The predictions from the model, which projected marked antibacterial suppression, found validation through our actual observations, particularly underscoring the potency of DES 3 and DES 4 at a molar ratio of 1:5. The ability of COSMO-RS in accurately depicting the dynamic between HDESs and bacterial cell membranes reinforces the model's predictive capability, essential for constructing green antibacterial solutions. Such a close match between the predicted antibacterial action and the actual observations gains further support from similar studies [47], wherein COSMO-RS elucidated the impact of salt hydrophobicity on the toxicological behavior of HDESs. Moreover, the solubility forecasts by COSMO-RS, as documented by Lotfi et al. [48], aligned well with their practical experiments, showcasing the model's dependability, as seen in its accurate prediction of acyclovir's solubility.

3.3.3. Synergistic Effect: MIC of antibiotic boosted with HDESs

To explore potential synergistic effects, DES 4 was combined with commercial antibiotics such as ampicillin, penicillin G and tetracycline, and the results detailing this synergistic impact, as assessed through MIC values, are provided in Table 6. Among the tested bacteria, DES 4 demonstrated the lowest MIC values against *S. aureus* and V. *vulnificus*, indicating its higher efficacy in inhibiting the growth of these bacteria. Interestingly, based on these results, the MIC values of the antibiotics combined with DES 4 were lower than the those of individual antibiotics, indicating that the boosted formulation possesses a higher potential for inhibitory activity against the same bacteria. These results were reflected in the enhanced MIC formulation values, ranging from 0.01 μg mL^{-1} to 0.02 μg mL^{-1}, compared to the MIC values of individual antibiotics alone, which ranged from 0.02 μg mL^{-1} to 2.5 μg mL^{-1} against the same bacteria. Noteworthy, when DES 4 was combined with tetracycline, it demonstrated an MIC value of 0.01 μg mL^{-1} for both bacterial strains. This outcome correlated with the previous MIC values,

Table 6
MIC values of ampicillin, penicillin G, and tetracycline combined with DES 3 and DES 4.

Minimum Inhibitory Concentration, MIC (in μg mL^{-1})[1,2]		
Ampicillin	*S. aureus*	*V. vulnificus*
	0.16	0.63
Penicillin	0.63	2.5
Tetracycline	0.16	1.25
DES 4	0.0440[2]	0.0440[2]
Ampicillin + DES 4	0.02	0.01
Penicillin + DES 4	0.01	0.02
Tetracycline + DES 4	0.01	0.01

[3]NA: Not applicable for the experimental purpose.
[4]Test included DMSO (10 μg mL^{-1}) as the negative control.
[1] Values are expressed in μg mL^{-1}, referring to the concentration of antibiotics; either in individual or in the synergistic effect.
[2] Values of DES were the best concentration obtained from the previous MIC result and were selected for the boosting MIC test.

Table 5
Minimum inhibitory concentrations (MICs) and minimum bactericidal concentrations (MBCs) of HDESs and individual counterparts.

	MIC					MBC				
Samples	DES 3	DES 4	Menthol	Octanoic acid	Decanoic acid	DES 3	DES 4	Menthol	Octanoic acid	Decanoic acid
Bacteria	Concentration (mg mL^{-1} %)[1]									
B. cereus	0.089	0.089	22.5	2.813	0.089	45	22.5	ND-	ND	ND
B. subtilis	0.176	0.044	ND	0.089	0.352	0.176	0.044	ND	0.089	0.352
C. diphtheria	1.406	5.625	ND	5.625	1.406	1.406	5.625	ND	5.625	1.406
C. perfringens	0.044	0.176	45	5.625	0.089	45	ND	ND	22.5	45
L. monocytogenes	0.352	0.176	0.089	0.176	0.176	0.352	0.176	0.703	0.176	0.176
S. aureus	2.813	0.044	ND	11.25	0.703	2.813	0.044	ND	11.25	0.703
S. *pneumoniae*	5.625	1.406	45	45	2.813	5.625	1.406	45	45	2.813
E. coli	0.089	45	45	0.044	22.5	0.089	45	45	0.044	22.5
P. mirabilis	45	1.406	5.625	ND	1.406	45	1.406	5.625	ND	1.406
S. enteritidis	0.044	5.625	22.5	0.044	0.044	0.044	5.625	22.5	0.044	0.044
S. sonnei	5.625	22.5	ND	45	1.406	5.625	22.5	ND	45	1.406
S. typhi	0.352	5.625	ND	2.813	0.352	0.352	5.625	ND	2.813	0.352
V. parahaemolyticus	22.5	0.044	45	45	1.406	22.5	0.044	45	45	1.406
V. vulnificus	22.5	0.044	ND	ND	5.625	22.5	0.044	ND	ND	5.625

[1] ND – Not detected.

which indicated that DES 4 had the best antimicrobial activity against various Gram-positive and Gram-negative bacteria, particularly *S. aureus* and *V. vulnificus*. Thus, this result indicates an improvement in the effectiveness of the antibiotic when used in combination with DES, with the combined formulation demonstrating lower MIC values than the antibiotics alone [49,50].

In conclusion, DES 4 serves as a potential antimicrobial agent to achieve remarkable antimicrobial enhancements by the synergistic effect on three types of first-line antibiotics: ampicillin, penicillin G and tetracycline. This result suggests that incorporating DES 4 into the antibiotics favorably enhanced the efficacy of the commercial and existing antibiotics, which was also reported in previous studies [49,51]. Several antimicrobial mechanisms may explain this. First, the HDES enhances the solubility of antibiotics, increasing antibiotic availability at the site of action and allowing greater penetration into bacterial cells [50]. Second, the HDES may disrupt the bacterial cell membrane or interfere with intracellular processes, thereby increasing antibiotic penetration and cellular uptake and enhancing the action of antibiotics [52]. Third, HDES may alter the cellular physiological environment of bacteria, such as changes in enzyme activity, affecting their metabolic processes and making them more susceptible to the action of antibiotics [53]. Fourth, HDES may interfere with bacterial resistance mechanisms by inhibiting efflux pumps, which are responsible for expelling antibiotics from the cells, thus preventing the development of resistance, and making the bacteria more susceptible to antibiotics [49,54]. Additionally, the disorganization of the bacterial cell membrane by HDESs may be due to the penetration of the substance into the lipid bilayers, which leads to bilayer reorganization while simultaneously allowing the passage of antibiotic substances [55].

3.4. FTIR spectroscopy analysis

To unravel the molecular interactions and structural characteristics, DES 4 was specifically selected for the FTIR analysis, owing to its antimicrobial efficacy, especially against S. *aureus*, as evidenced in the antimicrobial assays. The results obtained from the FTIR analysis, with a focus on the functional groups and their interactions within DES 4, were then correlated with the COSMO-RS predictions. This alignment between experimental findings and COSMO-RS predictions aids in determining how DES 4 may disrupt bacterial cell membranes can provides an insight into their antimicrobial properties.

The FTIR spectra for DES 4 demonstrated in Fig. 8 show a wide band in the range of 2800–3000 cm^{-1} with peaks at 2955.62 and 2924.69 cm^{-1} and an additional peak at 2855.29 cm^{-1} that can be attributed to the medium stretching of C–H bonds in alkyl groups. Multiple single peaks are also observed at 1711.56 cm^{-1}, representing the carbonyl group (C = O), as well as a peak at 1465.54 cm^{-1} representing C = C alkene aromatic group, along with a peak at 937.81 cm^{-1}, which shows that the sample contains an aromatic compound with an alkene group. Finally, the peak is observed at 1281.70 cm^{-1}, representing the presence of an amine functional group. Overall, the FTIR spectrum of DES 4 indicated the presence of various functional groups, including alkyls, carbonyls, alkene aromatics, and amines.

To emphasize the results, the considerable presence of alkyl functional groups in DES 4 significantly affects its physical properties, such as the melting point, owing to the length of the alkyl chain, which allows a higher chance of van der Waals attraction between the molecules [56]. Moreover, the long chain of the alkyl functional group, particularly provided by decanoic acid ($C_{10}H_{20}O_2$), has a direct impact on the antimicrobial activity of DES owing to the contribution of the carbon chain to the disruption of the cell membrane, which causes cell death without reducing selectivity [57]. The presence of the carbonyl functional group has an additional effect on antimicrobial activity due to the polarity of the chain containing an oxygen atom that is more electronegative than the carbon atom. The polarity of the DES is a factor that influences the interaction between the DES and microbial cells, causing cell disruption, and therefore, microbial inhibition [58]. Comparing *S. aureus* and *V. vulnificus,* tan evident reduction in the peak was observed at approximately 1400 cm^{-1} ($-CH_3$) [59], indicating an interaction between the bacteria and DES 4, which was more intense in *S. aureus.*

Furthermore, for both bacteria, the intensity of the peak from 3500 to 3250 cm^{-1} (–OH) [60] was severely reduced after treatment. The band at 3250 cm^{-1} is associated with the stretching vibrations of the O–H bonds in alcohols and carboxylic acids [61]. Hydrogen bonds between the water molecules and the surface of the bacterial cell could have been disrupted by the treatment, resulting in a decrease in the

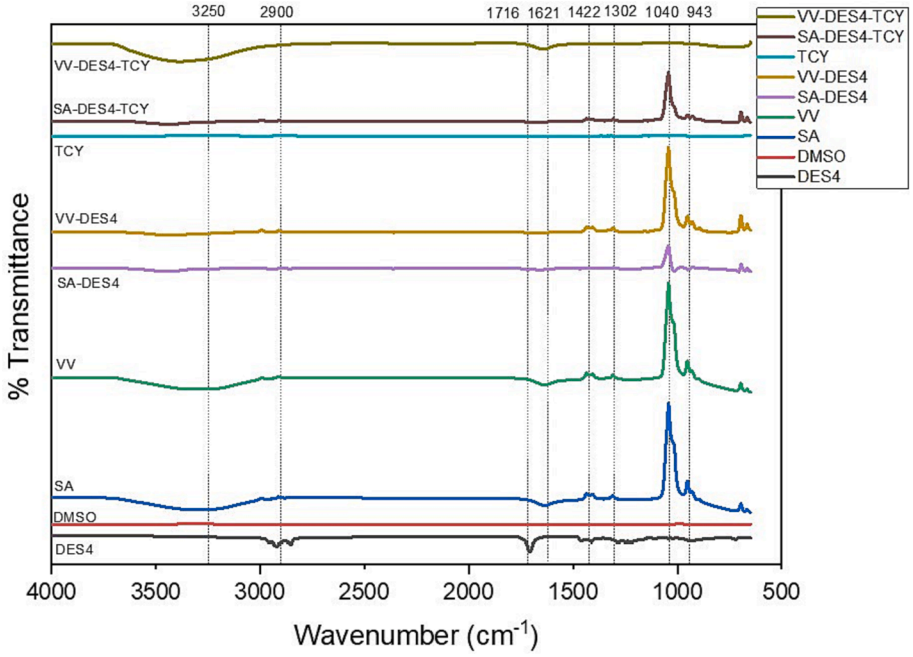

Fig. 8. Fourier transform infrared (FTIR) spectra for DES 4, DMSO (negative control), *S. aureus* (SA), *V. vulnificus* (VV), and their counterpart with DES 4 treatments, followed by the synergistic effect with tetracycline.

intensity of the –OH peak. Because of a change in the makeup or structure of the membrane, the loss of cell wall strength or the disruption of hydrogen bonding could potentially lead to the generation of reactive oxygen species. In addition, a change was observed at 1000–900 cm^{-1}, particularly at 1040 cm^{-1}, which associated with the bending vibrations of C–H bonds in aliphatic chains. Although the intensity reduced for both *S. aureus* and *V. vulnificus* after DES 4 treatments at 1050 cm^{-1}, it was more intense in *S. aureus,* which could be due to the different chemical compositions of the cell walls of the two bacterial species. The peak at 1050 cm^{-1} with C–O vibration was linked to carbohydrate or glycosidic linkages in the bacterial cell walls [62].

In Gram-positive bacteria, such as *S. aureus*, the cell wall is characterized by a thick layer of peptidoglycan, whereas Gram-negative bacteria, such as *V. vulnificus*, have a thinner layer of peptidoglycan and are surrounded by lipopolysaccharide, LPS-containing outer membranes. Therefore, the difference in intensity was most likely linked to the effect of DES 4 on the different cell membrane structures of the treated bacteria. The same reason could be applied to the strength of the peak at 970–900 cm^{-1}, which could be attributed to the disruption of phospholipids in both strains [63]. Owing to the dual nature of the phospholipid membrane, DES 4 hydrophobicity may cause dysfunction and cell rupture, which is supported by the FESEM results in the following section.

In conclusion, the lower peak intensity at 1040 cm^{-1} in *V. vulnificus* treated with tetracycline and HDESs compared to that in *S. aureus* suggested that HDESs may interfere with the metabolism of *V. vulnificus*, thus decreasing the number of aliphatic chains in the cell wall. Meanwhile, the higher peak intensity at 3250 cm^{-1} in the *S. aureus* samples treated with DES 4 suggested that DES 4 may increase the amount of alcohol in the cell wall [62]. HDESs might have varying impacts on the cell walls of diverse bacterial types. These differences in effect could stem from the distinct cell wall compositions found in various bacteria, such as those observed between Gram-negative and Gram-positive bacteria.

3.5. Examination of the antimicrobial activity using FESEM

To investigate the impact of DES 4 on bacterial broth samples and observe its influence on morphology, a series of studies using FESEM were conducted. Fig. 9a illustrates a control experiment with S. *aureus* in

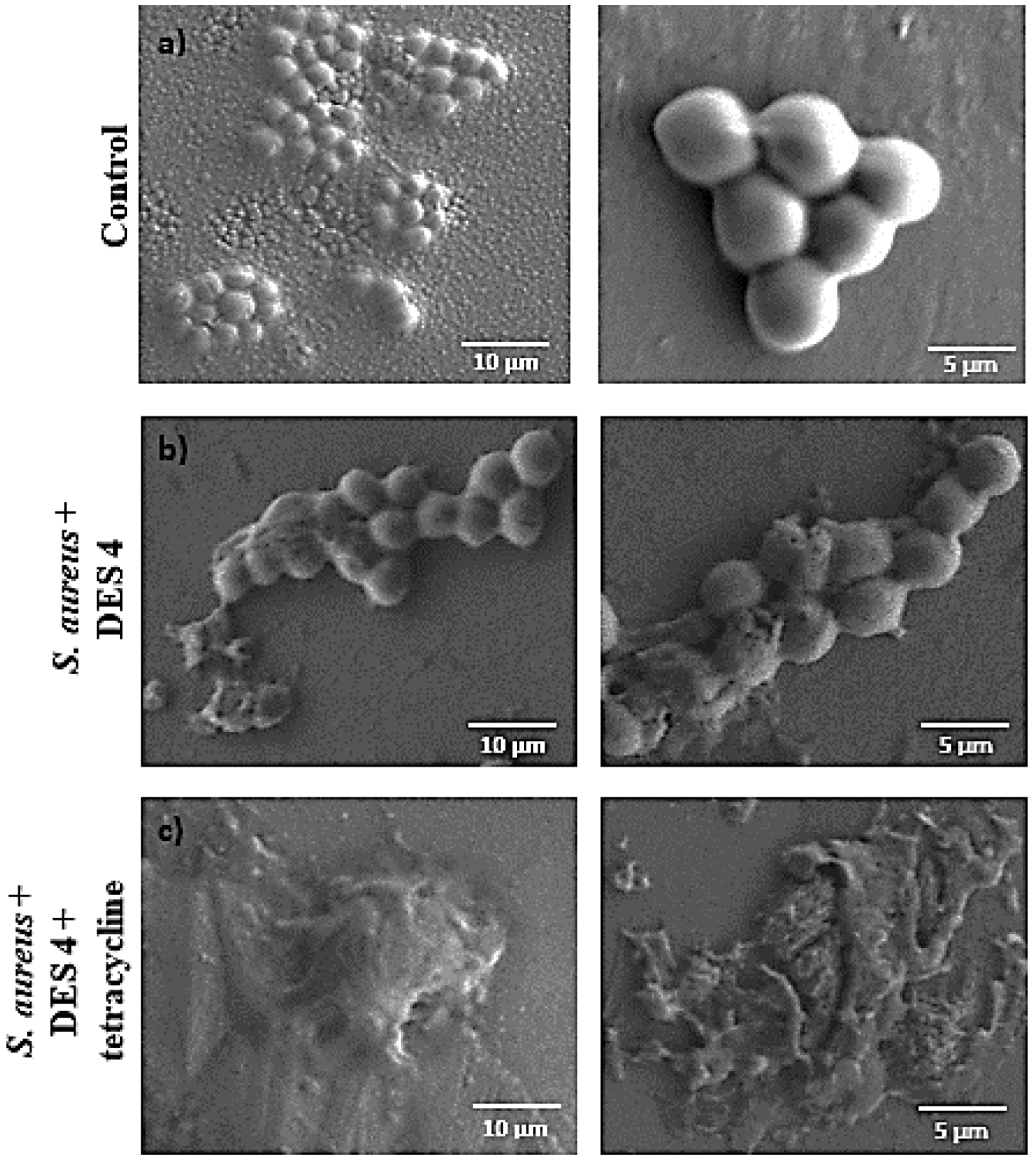

Fig. 9. FESEM images of *S. aureus* on samples that were (a) untreated (control), (b) treated with DES 4, and (c) treated with DES 4 and tetracycline at a magnification of 10 k and 5 k. Conditions: *S. aureus* was incubated at 37 °C for 24 h.

the absence of both DES 4 and tetracycline, while Fig. 9b and 9c depict *S. aureus* treated with DES 4 and a combination of DES 4 with tetracycline, respectively. These visuals provide insights into how DES 4 affects the structure of bacteria, connecting with the results obtained from FTIR and COSMO-RS analyses. The control group results (Fig. 9a) revealed the undisturbed circular cellular structure of the bacteria along with a polished exterior membrane. *S. aureus* was observed to adhere to untreated samples, as reported by Cao et al. [64]. However, after exposure to DES 4 (Fig. 9b) and DES 4 with tetracycline (Fig. 9c), bacterial membrane deformation and distortion in the shape of the microbial cells were visible and exhibited extensive perturbation, resulting in alterations in the shape of the microbial cells. Moreover, intracellular metabolites and cellular debris were detected in the surroundings, whereas DES 4 and tetracycline were present, suggesting a possible disruption of the cell membrane, leading to lysis. This result corresponds to the observations made in the FTIR analysis outlined in Section 3.4. In addition, both samples treated with DES 4 had the potential to prevent the survival of *S. aureus* and completely inhibit it owing to the presence of cations (menthol) and anions (decanoic acid) [65] as observed in COSMO-Rs prediction. According to Yoon et al. [30], antimicrobial lipids such as monoglycerides and FAs are potent antibacterial substances that can disrupt bacterial cell membranes. Similar findings have been reported by Pandit et al. [66] wherein the bacterial membrane was lost upon treatment with the peptide. In summary, according to the FESEM images, DES 4 appears to contribute to restraining bacterial activity when combined with common antibiotics like tetracycline.

4. Conclusion

The ability of the COSMO-RS model to predict the HDES interactions with bacterial cell membranes has the potential to validate the use of HDESs as environmentally friendly antibacterial agents, thereby reducing the need for extensive experimental testing. Thus, menthol-based HDESs exhibited potential as antibacterial agents. DES 4 (menthol:decanoic acid) showed superior inhibitory properties compared to DES 3 (menthol:octanoic acid) against Gram-positive and Gram-negative bacteria, with a larger inhibition zone against *L. monocytogenes*. Both HDESs effectively inhibited bacterial growth at various concentrations. Morphological and FTIR analyses confirmed the inhibitory effects of DES 4 on *S. aureus*, which caused membrane deformations and disruption of functional groups. Notably, the synergistic effects were observed when DES 4 is used in combination with conventional antibiotics. The potentiation of antibiotic performance by DES 4 enhanced its efficacy against bacterial strains and suggested a promising approach to combat antimicrobial resistance. This synergistic effect illustrates that the performance of antibiotics can be effectively enhanced, leading to lower antibiotic dosages, potentially mitigating side effects and the developmental resistance.

However, it is essential to extend this research to explore different arrays, including the screen of other bacteria strains and HDES formulations. Also, future research could focus on examining the toxicity and long-term effects of HDESs on human cells, performing *in vivo* experiments, and investigating the mechanisms of action of HDESs on bacterial membranes. Such studies could unlock possibilities for practical applications and offer a more thorough understanding of the potential and safety of HDESs as promising antibacterial agents.

Author contributions

A.A.M.E designed the research, obtained the fund and supervised; A. A.M.E, H.W.K., N.M.N., and S.S.S.P analyzed the data and wrote the manuscript. H.W.K., N.M.N., and E.N.E. performed the experiments. A.H analyzed data and validated the results. M.H. designed the research, analyzed data, validated results, and edited the manuscript. H.F.H. provided the software license COSMO-RS. M.S.A.S provided research resources and supervision. All the authors contributed to the manuscript and approved the submitted version. L.A. analyzed results. M.M. provided research resources and reviewed the manuscript. W.J.B. provided research resources for some analyses.

Funding

This work was supported by the Fundamental Research Grant Scheme (FRGS) [FRGS/1/2021/STG02/UIAM/03/1] by the Ministry of Higher Education, Malaysia.

CRediT authorship contribution statement

Amal A.M. Elgharbawy: . **Huma Warsi Khan:** Formal analysis, Writing – original draft, Writing – review & editing. **Najihah Mohd Noor:** Investigation, Writing – original draft. **Sharifah Shahira Syed Putra:** Writing – original draft, Writing – review & editing. **Engku Normi Engku Ismail:** Investigation. **Hanee Farzana Hizaddin:** Software. **Maan Hayyan:** Conceptualization, Formal analysis, Validation, Writing – review & editing. **Adeeb Hayyan:** Conceptualization, Validation. **Wan Jefrey Basirun:** Resources. **Muhammad Moniruzzaman:** Resources, Writing – review & editing. **Lama Al-afandi:** Formal analysis. **Muhamad Shirwan Abdullah Sani:** Resources, Writing – review & editing.

Declaration of competing interest

The authors declare that they have no known competing financial interests or personal relationships that could have appeared to influence the work reported in this paper.

Data availability

Data will be made available on request.

Acknowledgment

The authors express their gratitude to the Ministry of Higher Education in Malaysia for generously providing the grant to support this research. The authors sincerely appreciate the high-quality FESEM analysis provided by Mr. Mohd Shukri Aziz (Senior Assistant Science Officer), from the Chemistry Department, Faculty of Science, Universiti Malaya.

Appendix A. Supplementary data

Supplementary data to this article can be found online at https://doi.org/10.1016/j.molliq.2024.124008.

References

[1] B. Havenga, T. Ndlovu, T. Clements, B. Reyneke, M. Waso, W. Khan, Exploring the antimicrobial resistance profiles of WHO critical priority list bacterial strains, BMC Microbiol. 19 (2019) 1–16, https://doi.org/10.1186/s12866-019-1687-0.
[2] A. Hayyan, M.K. Hadj-Kali, M.Z.M. Salleh, M.A. Hashim, S.R. Rubaidi, M. Hayyan, M.Y. Zulkifli, S.N. Rashid, M.E.S. Mirghani, E. Ali, W.J. Basirun, Characterization of tetraethylene glycol-based deep eutectic solvents and their potential application for dissolving unsaturated fatty acids, J Mol Liq. 312 (2020) 113284, https://doi.org/10.1016/j.molliq.2020.113284.
[3] Z.-H. Cai, J.-D. Wang, L. Liu, L.-D. Ruan, Q.i. Gu, X.-Y. Yan, L.-N. Fu, P.-Q. Zhao, S. u. Zhang, Y.-J. Fu, A green and designable natural deep eutectic solvent-based supramolecular solvents system: Efficient extraction and enrichment for phytochemicals, Chem. Eng. J. 457 (2023) 141333, https://doi.org/10.1016/j.cej.2023.141333.
[4] T. Ahmad, J. Iqbal, M.A. Bustam, M. Babar, M.B. Tahir, M. Sagir, M. Irfan, H. M. Anwaar Asghar, A. Hassan, A. Riaz, L.F. Chuah, A. Bokhari, M. Mubashir, P. L. Show, Performance evaluation of phosphonium based deep eutectic solvents coated cerium oxide nanoparticles for CO_2 capture, Environ Res. 222 (2023) 115314, https://doi.org/10.1016/j.envres.2023.115314.
[5] M.H. Zainal-Abidin, M. Hayyan, W.F. Wong, Hydrophobic deep eutectic solvents: Current progress and future directions, J. Ind. Eng. Chem. 97 (2021) 142–162, https://doi.org/10.1016/j.jiec.2021.03.011.

[6] C.-C. Chen, Y.-H. Huang, S.-M. Hung, C. Chen, C.-W. Lin, H.-H. Yang, Hydrophobic deep eutectic solvents as attractive media for low-concentration hydrophobic VOC capture, Chem. Eng. J. 424 (2021) 130420, https://doi.org/10.1016/j.cej.2021.130420.

[7] P.A. Khan, S.K. Johl, S.K. Johl, Does adoption of ISO 56002–2019 and green innovation reporting enhance the firm sustainable development goal performance? An Emerging Paradigm, Bus Strategy Environ. 30 (2021) 2922–2936, https://doi.org/10.1002/bse.2779.

[8] P.A. Khan, S.K. Johl, S. Akhtar, M. Asif, A.A. Salameh, T. Kanesan, Open Innovation of Institutional Investors and Higher Education System in Creating Open Approach for SDG-4 Quality Education: A Conceptual Review, J. Open Innov. Technol. Mark. Complex. 8 (1) (2022) 49, https://doi.org/10.3390/joitmc8010049.

[9] K. Kongpol, N. Sermkaew, F. Makkliang, S. Khongphan, L. Chuaboon, A. Sakdamas, S. Sakamoto, W. Putalun, G. Yusakul, Extraction of curcuminoids and ar-turmerone from turmeric (*Curcuma longa* L.) using hydrophobic deep eutectic solvents (HDESs) and application as HDES-based microemulsions, Food Chem. 396 (2022) 133728, https://doi.org/10.1016/j.foodchem.2022.133728.

[10] J.M. Silva, E. Silva, R.L. Reis, A.R.C. Duarte, A closer look in the antimicrobial properties of deep eutectic solvents based on fatty acids, Sustain Chem Pharm. 14 (2019) 100192, https://doi.org/10.1016/j.scp.2019.100192.

[11] W. Chen, X. Li, L. Chen, G. Zhou, Q. Lu, Y. Huang, Y. Chao, W. Zhu, Tailoring hydrophobic deep eutectic solvent for selective lithium recovery from the mother liquor of Li_2CO_3, Chem. Eng. J. 420 (2021) 127648, https://doi.org/10.1016/j.cej.2020.127648.

[12] J. Wang, J. Xue, X. Dong, Q. Yu, S.N. Baker, M. Wang, H. Huang, Antimicrobial properties of benzalkonium chloride derived polymerizable deep eutectic solvent, Int J Pharm. 575 (2020) 119005, https://doi.org/10.1016/j.ijpharm.2019.119005.

[13] Q.Q. Koh, Y.L. Kua, S. Gan, K.W. Tan, T.Z.E. Lee, W.K. Cheng, H.L.N. Lau, Sugar-based natural deep eutectic solvent (NADES): Physicochemical properties, antimicrobial activity, toxicity, biodegradability and potential use as green extraction media for phytonutrients, Sustain Chem Pharm. 35 (2023) 101218, https://doi.org/10.1016/j.scp.2023.101218.

[14] T.R. Sekharan, R.M. Chandira, S. Tamilvanan, S.C. Rajesh, B.S. Venkateswarlu, Deep eutectic solvents as an alternate to other harmful solvents, Biointerface Res Appl Chem. 12 (2022) 847–860, https://doi.org/10.33263/BRIAC121.847860.

[15] A.S. Darwish, S.E.E. Warrag, T. Lemaoui, M.K. Alseiari, F.A. Hatab, R. Rafay, I. Alnashef, J. Rodríguez, N. Alamoodi, Green extraction of volatile fatty acids from fermented wastewater using hydrophobic deep eutectic solvents, Fermentation. 7 (2021) 226, https://doi.org/10.3390/fermentation7040226.

[16] M. Nakaoka, K.V.B. Tran, K. Yanase, H. Machida, K. Norinaga, Prediction of phase behavior of CO_2 absorbents using conductor-like screening model for real solvents (COSMO-RS): an approach to identify phase separation solvents of amine/ether/water systems upon CO_2 absorption, Ind Eng Chem Res. 59 (2020) 19020–19029.

[17] N. Islam, H.W. Khan, A.A. Gari, M. Yusuf, K. Irshad, Screening of ionic liquids as sustainable greener solvents for the capture of greenhouse gases using COSMO-RS approach: Computational study, Fuel. 330 (2022) 125540, https://doi.org/10.1016/j.fuel.2022.125540.

[18] S. Rezaei Motlagh, R. Harun, D. Awang Biak, S. Hussain, W. Wan Ab Karim Ghani, R. Khezri, C. Wilfred, A. Elgharbawy, Screening of Suitable Ionic Liquids as Green Solvents for Extraction of Eicosapentaenoic Acid (EPA) from Microalgae Biomass Using COSMO-RS Model, Molecules. 24 (4) (2019) 713, https://doi.org/10.3390/molecules24040713.

[19] X. Li, H. Gao, L.e. Zhou, Y.i. Nie, Screening Ionic Liquids by the COSMO-RS Method for the Preparation of Antibacterial Cellulose Fibers, ACS Sustain Chem Eng. 9 (46) (2021) 15525–15536.

[20] J.P. Wojeicchowski, A.M. Ferreira, D.O. Abranches, M.R. Mafra, J.A.P. Coutinho, Using COSMO-RS in the Design of Deep Eutectic Solvents for the Extraction of Antioxidants from Rosemary, ACS Sustain Chem Eng. 8 (2020) 12132–12141, https://doi.org/10.1021/acssuschemeng.0c03553.

[21] H.W. Khan, A.AM. Elgharbawy, M.U.H. Shah, B.M. Negash, M.K. Khan, K. Khan, H. Kamyab, M. Yusuf, Exploring Ionic Liquids for Formaldehyde Separation via Computational COSMO-RS Screening, Chemical Engineering Research and Design 196 (2023) 588–598, https://doi.org/10.1016/j.cherd.2023.06.055.

[22] M. Fallanza, M. González-Miquel, E. Ruiz, A. Ortiz, D. Gorri, J. Palomar, I. Ortiz, Screening of RTILs for propane/propylene separation using COSMO-RS methodology, Chem. Eng. J. 220 (2013) 284–293, https://doi.org/10.1016/j.cej.2013.01.052.

[23] W. Tang, Y. Dai, K.H. Row, Evaluation of fatty acid/alcohol-based hydrophobic deep eutectic solvents as media for extracting antibiotics from environmental water, Anal Bioanal Chem. 410 (2018) 7325–7336, https://doi.org/10.1007/s00216-018-1346-6.

[24] R. Verma, T. Banerjee, Palmitic-Acid-Based Hydrophobic Deep Eutectic Solvents for the Extraction of Lower Alcohols from Aqueous Media: Liquid-Liquid Equilibria Measurements, Validation and Process Economics, Global Challenges. 3 (2019) 1900024, https://doi.org/10.1002/gch2.201900024.

[25] M. Hayyan, Y.P. Mbous, C.Y. Looi, W.F. Wong, A. Hayyan, Z. Salleh, O. Mohd-Ali, Natural deep eutectic solvents: cytotoxic profile, Springerplus. 5 (2016), https://doi.org/10.1186/s40064-016-2575-9.

[26] M. Diedenhofen, A. Klamt, COSMO-RS as a tool for property prediction of IL mixtures-A review, Fluid Phase Equilib. 294 (2010) 31–38, https://doi.org/10.1016/j.fluid.2010.02.002.

[27] Q. Liu, J. Bi, X. Zhang, Effect of water on phenol separation from model oil with ionic liquids based on COSMO-RS calculation and experimental study, ACS Omega. 6 (41) (2021) 27368–27378.

[28] H. Cheng, C. Liu, J. Zhang, L. Chen, B. Zhang, Z. Qi, Screening deep eutectic solvents for extractive desulfurization of fuel based on COSMO-RS model, Chem. Eng. Process. Process Intensif. 125 (2018) 246–252, https://doi.org/10.1016/j.cep.2018.02.006.

[29] M. Goto, M. Moniruzzaman (Eds.), Application of Ionic Liquids in Drug Delivery, Springer Singapore, Singapore, 2021.

[30] B.K. Yoon, J.A. Jackman, E.R. Valle-González, N.-J. Cho, Antibacterial free fatty acids and monoglycerides: biological activities, experimental testing, and therapeutic applications, Int J Mol Sci. 19 (2018) 1114, https://doi.org/10.3390/ijms19041114.

[31] H.O.M. Abakar, S.E. Bakhiet, R.S.M. Abadi, Antimicrobial activity and minimum inhibitory concentration of *Aloe vera* sap and leaves using different extracts, J. Pharmacogn. Phytochem. 6 (2017) 298–303.

[32] S. Joardar, M.L. Adams, R. Biswas, G.V. Deodhar, K.E. Metzger, K. Deweese, M. Davidson, R.M. Richards, B.G. Trewyn, P. Biswas, Direct synthesis of silver nanoparticles modified spherical mesoporous silica as efficient antibacterial materials, Microporous Mesoporous Mater. 313 (2021) 110824, https://doi.org/10.1016/j.micromeso.2020.110824.

[33] A. Chakrabarti, Phospholipid asymmetry in biological membranes: is the role of phosphatidylethanolamine underappreciated? J Membr Biol. 254 (2) (2021) 127–132.

[34] A.S. Kooner, Y. Yuan, H. Yu, H. Kang, L. Klenow, R. Daniels, X. Chen, Sialosides Containing 7-N-Acetyl Sialic Acid Are Selective Substrates for Neuraminidases from Influenza A Viruses, ACS Infect Dis. 9 (2023) 33–41, https://doi.org/10.1021/acsinfecdis.2c00502.

[35] Y. Liu, Z. Qin, C. Wang, Z. Jiang, N-acetyl-d-glucosamine-based oligosaccharides from chitin: Enzymatic production, characterization and biological activities, Carbohydr Polym. 315 (2023) 121019, https://doi.org/10.1016/j.carbpol.2023.121019.

[36] H.a. Chin Ting, H. Warsi Khan, A. Vijaya Bhaskar Reddy, M. Goto, M. Moniruzzaman, Extraction of salicylic acid from wastewater using ionic liquid-based green emulsion liquid membrane: COSMO-RS prediction and experimental verification, J Mol Liq. 347 (2022) 118280, https://doi.org/10.1016/j.molliq.2021.118280.

[37] H.W. Khan, A.A.M. Elgharbawy, A. Bustam, M. Moniruzzaman, Design and Selection of Ionic Liquids Via COSMO for Pharmaceuticals and Medicine, in: M. Goto, M. Moniruzzaman (Eds.), Application of Ionic Liquids in Drug Delivery, Springer Singapore, Singapore, 2021, pp. 137–164.

[38] A. Mouffok, D. Bellouche, I. Debbous, A. Anane, Y. Khoualdia, A. Boublia, A. S. Darwish, T. Lemaoui, Y. Benguerba, Synergy of garlic extract and deep eutectic solvents as promising natural Antibiotics: Experimental and COSMO-RS, J Mol Liq. 375 (2023) 121321, https://doi.org/10.1016/j.molliq.2023.121321.

[39] H.W. Khan, A.A.M. Elgharbawy, M.A. Bustam, M. Goto, M. Moniruzzaman, Ionic liquid-based green emulsion liquid membrane for the extraction of the poorly soluble drug ibuprofen, Molecules. 28 (5) (2023) 2345, https://doi.org/10.3390/molecules28052345.

[40] H.W. Khan, A.V.B. Reddy, M.M.E. Nasef, M.A. Bustam, M. Goto, M. Moniruzzaman, Screening of ionic liquids for the extraction of biologically active compounds using emulsion liquid membrane: COSMO-RS prediction and experiments, J Mol Liq. 309 (2020) 113122, https://doi.org/10.1016/j.molliq.2020.113122.

[41] C. Jiang, H. Cheng, Z. Qin, R. Wang, L. Chen, C. Yang, Z. Qi, X. Liu, COSMO-RS prediction and experimental verification of 1,5-pentanediamine extraction from aqueous solution by ionic liquids, Green, Energy and Environment. 6 (2021) 422–431, https://doi.org/10.1016/j.gee.2020.12.011.

[42] H. Lu, Z. Yang, M. Yu, N. Ji, L. Dai, X. Dong, L. Xiong, Q. Sun, Characterization of complexes formed between debranched starch and fatty acids having different carbon chain lengths, Int J Biol Macromol. 167 (2021) 595–604, https://doi.org/10.1016/j.ijbiomac.2020.11.198.

[43] S. Rezaei Motlagh, R. Harun, D. Awang Biak, S.A.H. Radiah, Screening of Long Chain Imidazolium Base Ionic Liquids for EPA and DHA Extraction from Microalgae Using COSMO-RS Model 1 (2019) 23–29.

[44] T. Watanabe, Y. Yamamoto, M. Miura, H. Konno, S. Yano, Systematic Analysis of Selective Bactericidal Activity of Fatty Acids against *Staphylococcus aureus* with Minimum Inhibitory Concentration and Minimum Bactericidal Concentration, J Oleo Sci. 296 (2019) 291–296.

[45] G. Zu, M. Steinmüller, D. Keskin, H.C. van der Mei, O. Mergel, P. van Rijn, Antimicrobial nanogels with nanoinjection capabilities for delivery of the hydrophobic antibacterial agent triclosan, ACS Appl Polym Mater. 2 (12) (2020) 5779–5789.

[46] K. Radošević, I. Čanak, M. Panić, K. Markov, M.C. Bubalo, J. Frece, V.G. Srček, I. R. Redovniković, Antimicrobial, cytotoxic and antioxidative evaluation of natural deep eutectic solvents, Environ. Sci. Pollut. Res. 25 (14) (2018) 14188–14196.

[47] Y.P.V. Mbous, M. Hayyan, W.F. Wong, A. Hayyan, C.Y. Looi, M.A. Hashim, Simulation of Deep Eutectic Solvents' Interaction with Membranes of Cancer Cells using COSMO-RS, J Phys Chem b. (2020). https://api.semanticscholar.org/CorpusID:221721046.

[48] M. Lotfi, M. Moniruzzaman, M. Sivapragasam, S. Kandasamy, M.I. Abdul Mutalib, N.B. Alitheen, M. Goto, Solubility of acyclovir in nontoxic and biodegradable ionic liquids: COSMO-RS prediction and experimental verification, J Mol Liq. 243 (2017) 124–131, https://doi.org/10.1016/j.molliq.2017.08.020.

[49] S.N. Pedro, A.T.P.C. Gomes, P. Oskoei, H. Oliveira, A. Almeida, M.G. Freire, A.J. D. Silvestre, C.S.R. Freire, Boosting antibiotics performance by new formulations with deep eutectic solvents, Int J Pharm. 616 (2022) 121566, https://doi.org/10.1016/j.ijpharm.2022.121566.

[50] F. Al-Akayleh, R.M. Khalid, D. Hawash, E. Al-Kaissi, I.S.I. Al-Adham, N. Al-Muhtaseb, N. Jaber, M. Al-Remawi, P.J. Collier, Antimicrobial potential of natural deep eutectic solvents, Lett Appl Microbiol. 75 (3) (2022) 607–615, https://doi.org/10.1111/lam.13699.

[51] K. Cherkashina, A. Pochivalov, V. Simonova, F. Shakirova, A. Shishov, A. Bulatov, A synergistic effect of hydrophobic deep eutectic solvents based on terpenoids and carboxylic acids for tetracycline microextraction, Analyst. 146 (2021) 3449–3453, https://doi.org/10.1039/D1AN00096A.
[52] C. Prudêncio, M. Vieira, S. Van Der Auweraer, R. Ferraz, Recycling Old Antibiotics with Ionic Liquids, Antibiotics. 9 (2020) 1–16, https://doi.org/10.3390/antibiotics9090578.
[53] I. Juneidi, M. Hayyan, M.A. Hashim, Evaluation of toxicity and biodegradability for cholinium-based deep eutectic solvents, RSC Adv. 5 (2015) 83636–83647, https://doi.org/10.1039/c5ra12425e.
[54] D.D. Yang, N.J. Paterna, A.S. Senetra, K.R. Casey, P.D. Trieu, G.A. Caputo, T. D. Vaden, B.R. Carone, Synergistic interactions of ionic liquids and antimicrobials improve drug efficacy, Iscience. 24 (1) (2021) 101853, https://doi.org/10.1016/j.isci.2020.101853.
[55] M. Zakrewsky, A. Banerjee, S. Apte, T.L. Kern, M.R. Jones, R.E. Del Sesto, A. T. Koppisch, D.T. Fox, S. Mitragotri, Choline and Geranate Deep Eutectic Solvent as a Broad-Spectrum Antiseptic Agent for Preventive and Therapeutic Applications, Adv Healthc Mater. 5 (2016) 1282–1289, https://doi.org/10.1002/adhm.201600086.
[56] S.J. Bryant, A.J. Christofferson, T.L. Greaves, C.F. McConville, G. Bryant, A. Elbourne, Bulk and interfacial nanostructure and properties in deep eutectic solvents: Current perspectives and future directions, J Colloid Interface Sci. 608 (2022) 2430–2454, https://doi.org/10.1016/J.JCIS.2021.10.163.
[57] T. Shen, L. Chen, Y. Liu, S. Shi, Z. Liu, K. Cai, C. Liao, C. Wang, Decanoic acid modification enhances the antibacterial activity of PMAP-23RI-Dec, Eur. J. Pharm. Sci. 157 (2021) 105609, https://doi.org/10.1016/j.ejps.2020.105609.
[58] S. Javan bakht Dalir, H. Djahaniani, F. Nabati, M. Hekmati, Characterization and the evaluation of antimicrobial activities of silver nanoparticles biosynthesized from *Carya illinoinensis* leaf extract, Heliyon. 6 (3) (2020) e03624, https://doi.org/10.1016/j.heliyon.2020.e03624.
[59] W.F. Edgell, C.H. Ward, The Raman and Infrared Spectra of Tin Tetramethyl[1], J Am Chem Soc. 77 (1955) 6486–6491, https://doi.org/10.1021/ja01629a014.
[60] S. Shin, Y. Kim, J.H. Jin, J. Jung, Heat-Induced Dry Hydrolysis of Sodium Borohydride/Oxalic Acid Dihydrate Composite for Hydrogen Production, ACS Omega. 7 (2022) 979–986, https://doi.org/10.1021/acsomega.1c05571.
[61] M.G. Vazquez de Vasquez, K.A. Carter-Fenk, L.M. McCaslin, E.E. Beasley, J. B. Clark, H.C. Allen, Hydration and Hydrogen Bond Order of Octadecanoic Acid and Octadecanol Films on Water at 21 and 1 °C, J Phys Chem a. 125 (2021) 10065–10078, https://doi.org/10.1021/acs.jpca.1c06101.
[62] T. Hong, J.-Y. Yin, S.-P. Nie, M.-Y. Xie, Applications of infrared spectroscopy in polysaccharide structural analysis: Progress, challenge and perspective, Food Chem x. 12 (2021) 100168, https://doi.org/10.1016/j.fochx.2021.100168.
[63] A.P. Fellows, M.T.L. Casford, P.B. Davies, In situ investigation of the oxidation of a phospholipid monolayer by reactive oxygen species, Biophys J 122 (11) (2023) 2007–2022, https://doi.org/10.1016/j.bpj.2022.10.040.
[64] P. Cao, Y. Yang, F. Uche, S. Hart, W.-W. Li, C. Yuan, Coupling plant-derived cyclotides to metal surfaces: An antibacterial and antibiofilm study, Int J Mol Sci. 19 (3) (2018) 793, https://doi.org/10.3390/ijms19030793.
[65] K. Saikia, Y.D. Sravani, V. Ramakrishnan, N. Chaudhary, Highly potent antimicrobial peptides from N-terminal membrane-binding region of *E. coli* MreB, Sci Rep. 7 (2017) 1–9, https://doi.org/10.1038/srep42994.
[66] G. Pandit, N. Chowdhury, S. Abdul Mohid, A.P. Bidkar, A. Bhunia, S. Chatterjee, Effect of Secondary Structure and Side Chain Length of Hydrophobic Amino Acid Residues on the Antimicrobial Activity and Toxicity of 14-Residue-Long de novo AMPs, ChemMedChem. 16 (2020) 355–367, https://doi.org/10.1002/cmdc.202000550.